

state resistivity =  $5.7 \times 10^{-6} \Omega\text{cm}$ ,  $\gamma = 1.1 \times 10^4 \text{ ergs/cm}^3 (\text{K}^\circ)^2$ , and  $(S/S_f)$  is the ratio of the free Fermi surface area to that of a corresponding free electron gas. Making the usual<sup>10,11</sup> rather uncertain assumption  $(S/S_f) \approx 0.6$  for transition metals, Eq. (6) yields  $\kappa \approx 0.86 + 4.49 = 5.35$  in fair agreement with the  $\kappa$  values based on Eq. (5) and listed in Table I.

(3). *High-field energy gap.* According to Abrikosov<sup>7</sup> the high-field superconducting state consists of a regular lattice of quantized supercurrent vortices over which the field-dependent Ginzburg-Landau order parameter [hence BCS energy gap  $\epsilon(H)$ <sup>8,20</sup>] varies, becoming zero only along (zero-volume) lines at the center of each vortex where  $H$  is a maximum. The high-field superconducting-state electronic specific heat  $C_{es}(T, H)$  might then be expected to reflect a spatially averaged gap  $\bar{\epsilon}(H)$  which diminishes with increasing  $H$ , as is indeed implied by the observed  $C_{es}(T, H)$  of Eq. (1) since  $\bar{\epsilon}(H) \approx 2b(H)kT_s(H)$ ,<sup>21</sup> where  $k$  is the Boltzmann constant. In analogy with the case of pure element gap anisotropy in momentum space,<sup>22,23</sup> one might expect the smaller

gap regions in real space (assuming Abrikosov's model<sup>7</sup>) to dominate  $C_{es}(T, H \gg 0)$  at very low reduced temperature, producing considerable upward curvature in the plots of Fig. 3 at higher  $(T_s/T)$ , as is also suggested by the entropy considerations above, and which might account for the failure of the  $\text{V}_3\text{Ga}^1$  high-field  $(C/T)$  versus  $T^2$  curves to extrapolate to 0 at  $T^2 = 0$ .

*Note added in proof.* For a derivation of entropy, Gibbs free energy, and magnetization from the present specific-heat data see R. R. Hake, *Rev. Mod. Phys.* **36**, 124 (1964). The magnetization and its relationship to the effective field-dependent energy gap (as inferred from the exponential temperature dependence of the high-field superconducting-state electronic specific heat) appear to be in reasonable accord with the GLAG theory.

#### ACKNOWLEDGMENTS

We wish to thank D. M. Sellman and H. Nadler for specimen preparation, C. G. Rhodes for micrographic examinations, and K. Medeiros for computer programming. Valuable discussions with T. G. Berlincourt, D. Kramer, H. B. Levine, and H. W. Wiedersich are gratefully acknowledged.

<sup>21</sup> See, for example, E. A. Lynton, *Superconductivity* (Methuen and Company, Ltd., London, 1962), p. 84.

<sup>22</sup> L. N. Cooper, *Phys. Rev. Letters* **3**, 17 (1959).

<sup>23</sup> P. W. Anderson, *J. Phys. Chem. Solids* **11**, 26 (1959).

## Faraday Rotation of Rare-Earth (III) Phosphate Glasses

S. B. BERGER,† C. B. RUBINSTEIN, C. R. KURKJIAN, AND A. W. TREPTOW  
*Bell Telephone Laboratories, Murray Hill, New Jersey*

(Received 25 April 1963; revised manuscript received 17 September 1963)

The optical Faraday rotation of trivalent rare-earth phosphate glasses has been investigated at room temperature. The rotation is ascribed primarily to strong electric dipole transitions involving the rare-earth 4f electrons and is described as a function of the incident light wavelength by a simplified equation involving an effective transition wavelength. The linear dependence of the rotation on the concentration is experimentally demonstrated. The relative magnitudes of the magnetic rotation of the rare-earth ions are compared to the quantity  $p^2/g$ , where  $p$  is the effective magneton number and  $g$  is the spectroscopic splitting factor. This comparison demonstrates the importance of the other parameters, especially the transition wavelengths and electric dipole matrix elements. It also indicates that a prediction of relative rotations of ions, molecules, etc., on the basis of relative magnitudes of magnetic susceptibility and concentration alone is not meaningful.

#### INTRODUCTION

**F**ARADAY rotation of some rare-earth ions has been extensively studied at Leiden University, especially by J. Becquerel, in the first half of this century.<sup>1</sup> The object of that effort was to understand the phenomena of Faraday rotation with particular respect to its wavelength dependence, temperature dependence, and relation to the magnetic susceptibility.

The object of this paper is to present the room-temperature optical Faraday rotation of all the trivalent rare-earth ions (except  $\text{Pm}^{3+}$ ) in the isotropic phosphate glass matrix as a function of wavelength and concentration in order to furnish a basis for numerical comparison of the magnetic rotatabilities of the trivalent rare-earth ions. The results indicate that the relative magnitudes of the observed rotations bear no simple relation to any one parameter. For example, the magnetic susceptibility is shown not to be a suitable basis for the prediction of the relative rotations. However, the experimental evidence is that the wavelength

† Present address: RCA Laboratories, Princeton, New Jersey.

<sup>1</sup> Communications Kamerlingh Onnes Laboratory, Leiden University, especially during the period 1925-1936.

dependence of the Faraday rotation for an individual rare-earth ion may be expressed simply in terms of an effective transition wavelength, a fact of some importance which will be discussed.

### EXPERIMENTAL

The phosphate glass system was selected in view of the advantageous properties of optical isotropy and ease of fabrication. Alers<sup>2</sup> made use of this matrix in his field dependence investigation of the magnetic rotation of cerous phosphate glass at liquid-helium temperatures. The samples used in this study were prepared of approximately the metaphosphate composition:  $R(\text{PO}_3)_3$ , which may also be expressed as  $R_2\text{O}_3 \cdot 3\text{P}_2\text{O}_5$ , where  $R$  represents the rare-earth ion. These samples were analyzed and the ratio of  $\text{P}_2\text{O}_5$  to  $R_2\text{O}_3$ , designated as  $x$ , was calculated. The density (measured by a buoyancy method), color, number of rare-earth ions per  $\text{cm}^3$   $N$  (determined by computing a formula weight per mole rare-earth ion from the chemical analysis) and  $x$  are tabulated in Table I.

TABLE I. Physical properties and composition of the trivalent rare-earth phosphate glasses.

$R$	Visual appearance	Density $\text{g/cm}^3$	$x$	$N(\times 10^{-21})$ $\frac{R \text{ ions}}{\text{cm}^3}$
Ce	Pale yellow to colorless <sup>a</sup>	3.54	$2.67 \pm 0.08$	$6.0 \pm 0.1$
Pr	Green	3.37	3.09	5.3
Nd	Purple	3.48	2.92	5.6
Sm	Yellow	3.45	2.87	5.5
Eu	Pale peach	3.47	2.93	$5.4_5$
Gd	Colorless	3.48	3.01	5.3
Tb	Colorless	3.52	2.94	5.4
Dy	Pale yellow	3.76	2.51	6.2
Ho	Golden yellow	3.58	2.94	5.4
Er	Pink	3.59	3.01	$5.3_5$
Tm	Pale green	3.75	2.79	5.8
Yb	Colorless	3.89	3.01	5.7

<sup>a</sup> Yellow color attributed to  $\text{Ce}^{4+}$  ion.

### WAVELENGTH DEPENDENCE

The magnetic rotation produced by a material is usually expressed in terms of the Verdet constant  $V$  (in units of minutes of arc per cm path length per oersted) which is defined by the equation

$$\theta = V H d, \quad (1)$$

where  $\theta$  is the rotation of the plane of polarization of linearly polarized light produced by the action of the longitudinal magnetic field  $H$  on a material of optical path length  $d$ . Except for localized variations produced about the wavelengths of the weak, intra-f-orbital transitions, the Verdet constant of these materials may be described by the equation

$$V = K(\lambda^2 - \lambda_t^2)^{-1}, \quad (2)$$

<sup>2</sup> P. Alers, Phys. Rev. **116**, 1483 (1959).

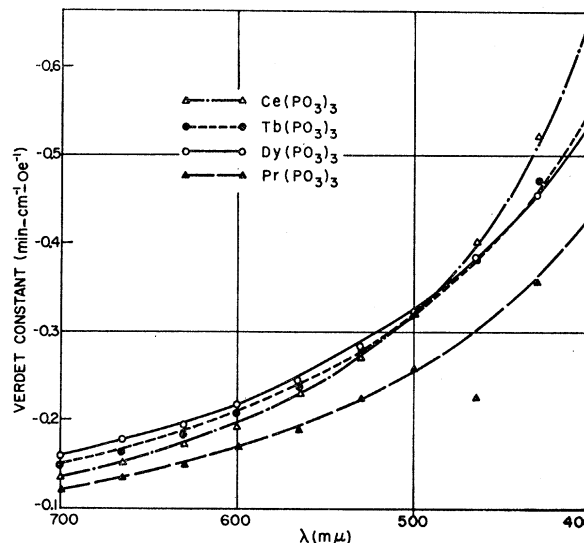


Fig. 1. Verdet constant as a function of incident light wavelength for  $\text{Ce}^{3+}$ ,  $\text{Pr}^{3+}$ ,  $\text{Tb}^{3+}$ , and  $\text{Dy}^{3+}$  phosphate glasses at room temperature. The curves represent Eq. (2), and the circles and triangles the experimental points.

where  $K$  is a parameter independent of the incident light's wavelength  $\lambda$ , but a function, among other things, of the transition wavelength  $\lambda_t$ , effective electric dipole matrix element  $C_t$ , temperature and concentration. The wavelength dependence of this equation is well known and corresponds to paramagnetic type rotation,<sup>3</sup> but the equation is not general in that it is predicated on the assumption that the transitions which give rise to the Faraday rotation may be represented as a single effective transition at  $\lambda_t$ . The wavelength  $\lambda_t$  represents a weighted average of the actual transition wavelengths and reflects the relative strength of the transitions and the proximity of the actual transition frequencies to the observing frequency (obviously, for transitions of the same strength, the closer transitions will be the more important). The value of  $\lambda_t$  is straightforward when only one transition is dominant. However, when several transitions are involved,  $\lambda_t$  serves as an indicator of the spectral region in which the transitions are located.

Figure 1 contains a plot of the measured wavelength variation, using a  $6\text{-m}\mu$  bandpass, of the Verdet constant in the visible spectral region for  $\text{Ce}^{3+}$ ,  $\text{Pr}^{3+}$ ,  $\text{Tb}^{3+}$ , and  $\text{Dy}^{3+}$  phosphate, the four strongest Faraday rotating, phosphate glasses. The curves are fitted to Eq. (2) with a  $\lambda_t$  of  $289\text{ m}\mu$  for  $\text{Ce}^{3+}$ ,  $210\text{ m}\mu$  for  $\text{Pr}^{3+}$ ,  $215\text{ m}\mu$  for  $\text{Tb}^{3+}$ , and  $175\text{ m}\mu$  for  $\text{Dy}^{3+}$ . In Fig. 1, the point at  $465\text{ m}\mu$  for  $\text{Pr}^{3+}$  phosphate which grossly deviates from the curve occurs near the positions of intra-f-orbital transitions.

In order to understand the significance of these  $\lambda_t$  values, one must study the ultraviolet absorption

<sup>3</sup> J. H. Van Vleck, *Electric and Magnetic Susceptibilities* (Oxford University Press, London, 1932), p. 368.

TABLE II. Measured Verdet constants of trivalent rare-earth phosphate glasses at various wavelengths in the visible spectral region.

Wave-length	Verdet constant—trivalent rare-earth ion												
	La	Ce	Pr	Nd	Sm	Eu	Gd	Tb	Dy	Ho	Er	Tm	Yb
405 <sup>a</sup>	0.037 <sub>1</sub>	-0.672	-0.447	-0.250	0.026 <sub>3</sub>	-0.025	0.018 <sub>2</sub>	-0.560	-0.540	-0.299	-0.139	0.019 <sub>7</sub>	0.087 <sub>9</sub>
420	0.033 <sub>5</sub>	-0.585	-0.395	-0.227	0.026 <sub>2</sub>	-0.021	0.016 <sub>9</sub>	-0.501	-0.494	-0.281	-0.127	0.017 <sub>4</sub>	0.077 <sub>6</sub>
436 <sup>a</sup>	0.030 <sub>4</sub>	-0.510	-0.332	-0.209	0.024 <sub>4</sub>	-0.017	0.015 <sub>7</sub>	-0.458	-0.453	-0.313	-0.121	0.013 <sub>3</sub>	0.072 <sub>9</sub>
450	0.029 <sub>0</sub>	-0.459	-0.338	-0.197	0.023 <sub>7</sub>	-0.016	0.015 <sub>6</sub>	-0.419	-0.419	-0.315	-0.120	0.011 <sub>2</sub>	0.065 <sub>3</sub>
465	0.025 <sub>9</sub>	-0.403	-0.283	-0.183	0.022 <sub>0</sub>	-0.016	0.015 <sub>0</sub>	-0.385	-0.388	-0.135	-0.111	0.011 <sub>3</sub>	0.061 <sub>6</sub>
480	0.024 <sub>7</sub>	-0.366	-0.283	-0.167	0.020 <sub>9</sub>	-0.010	0.014 <sub>5</sub>	-0.357	-0.359	-0.156	-0.100	0.012 <sub>1</sub>	0.056 <sub>3</sub>
500	0.022 <sub>6</sub>	-0.326	-0.261	-0.155	0.020 <sub>4</sub>	-0.006	0.012 <sub>8</sub>	-0.323	-0.331	-0.153	-0.111	0.009 <sub>6</sub>	0.050 <sub>7</sub>
520	0.020 <sub>6</sub>	-0.287	-0.236	-0.136	0.017 <sub>4</sub>	-0.006	0.012 <sub>1</sub>	-0.295	-0.301	-0.138	-0.095	0.008 <sub>2</sub>	0.045 <sub>0</sub>
546 <sup>a</sup>	0.018 <sub>7</sub>	-0.253 <sub>5</sub>	-0.208	-0.134	0.015 <sub>6</sub>	-0.005	0.011 <sub>5</sub>	-0.261	-0.268	-0.138	-0.062	0.006 <sub>6</sub>	0.041 <sub>3</sub>
578 <sup>a</sup>	0.015 <sub>7</sub>	-0.217	-0.182	-0.094	0.014 <sub>4</sub>	-0.004	0.011 <sub>0</sub>	-0.226	-0.237	-0.119	-0.060	0.005 <sub>5</sub>	0.036 <sub>2</sub>
600	0.014 <sub>9</sub>	-0.197	-0.170	-0.080	0.012 <sub>4</sub>	-0.003	0.010 <sub>3</sub>	-0.206	-0.217	-0.110	-0.057	0.004 <sub>3</sub>	0.032 <sub>3</sub>
635	0.013 <sub>5</sub>	-0.173	-0.150	-0.080	0.011 <sub>7</sub>	-0.002	0.009 <sub>3</sub>	-0.190	-0.197	-0.098	-0.051	0.004 <sub>4</sub>	0.029 <sub>4</sub>
670		-0.150	-0.132	-0.071	0.010 <sub>0</sub>	-0.002	0.009 <sub>0</sub>	-0.164	-0.173	-0.084	-0.044	0.007 <sub>2</sub>	0.024 <sub>3</sub>
700	0.011	-0.132	-0.123	-0.056	0.009 <sub>0</sub>		0.008 <sub>9</sub>	-0.150	-0.159	-0.077	-0.040	0.001 <sub>7</sub>	0.022 <sub>3</sub>

<sup>a</sup> Mercury spectral lines.

spectra of the trivalent rare-earth phosphate glasses. Experimental limitations, have restricted this investigation to only cerous phosphate glass for which absorption peaks are observed at 294 and 245 m $\mu$  in addition to a much smaller peak at 227 m $\mu$  which has been reported elsewhere.<sup>4</sup> The peak at 294 m $\mu$  is about an order of magnitude more intense than the one at 245 m $\mu$ , a fact which is in agreement with the indication that the rotation is primarily produced by the transition at 294 m $\mu$ . This transition is presumably that of the lone 4*f* electron to the 5*d* shell or, more specifically, the transition from the <sup>2</sup>F<sub>5/2</sub> ground state to the crystal field split <sup>2</sup>D<sub>3/2,5/2</sub>. Absorption spectra for rare-earth ions have been observed in solution. For example, Ce<sup>3+</sup>, Pr<sup>3+</sup>, Tb<sup>3+</sup>, and Dy<sup>3+</sup> have been observed as the bromide complex in ethanol solution.<sup>5</sup> Absorption peaks at 314 m $\mu$  for Ce<sup>3+</sup>, 225 m $\mu$  for Pr<sup>3+</sup>, 230.5 m $\mu$  for Tb<sup>3+</sup>, and less than 205 m $\mu$  for Dy<sup>3+</sup> have been reported. In addition the aquo complexes of Pr<sup>3+</sup> and Tb<sup>3+</sup> in ethanol show absorption bands at 215 and 220 m $\mu$ , respectively. These bands have been identified as arising from the transition of a 4*f* electron to the 5*d* shell. In comparing these wavelengths to the values of  $\lambda_i$  stated previously, a close correspondence is noted. From the magnitude of the rotation, one may conclude that these absorptions do indeed arise from an allowed electric dipole transition, indicating that the assignment is reasonable.

The rotation for the other rare-earth ion phosphates is significantly smaller. The corresponding increase in experimental error, which results from the decrease in rotation, and in some cases several interfering, visible absorption lines make equation fitting dubious. However, it may be said that the general shape of the curves of Verdet constant as a function of wavelength is consistent with Eq. (2). For small rotations the contribution of the matrix must be considered. This contribution will have a different wavelength dependence;

but since the transition producing this rotation is in the vacuum ultraviolet, the wavelength dependence will not appear significantly different than that of Eq. (2). Table II contains a compilation of the measured values of the Verdet constant in the visible spectral region for all the rare-earth glasses measured.

#### CONCENTRATION DEPENDENCE

Several mixtures of two or more rare-earth ions in a glass matrix were investigated to corroborate the expectation that the Verdet constant is a linear function of *N* at the high concentrations employed. In one specific case to be discussed here, measurements were made at room temperature on various Ce<sup>3+</sup>-Nd<sup>3+</sup> mixtures in a phosphate glass. The Verdet constant of the mixture is assumed to be a linear function of the respective rare-earth ion concentrations, i.e.,

$$V = aV_1 + (1-a)V_2, \quad (3)$$

where *a* and (1-*a*) are the mole fractions of Ce(PO<sub>3</sub>)<sub>3</sub> and Nd(PO<sub>3</sub>)<sub>3</sub>, respectively, and *V*, *V*<sub>1</sub>, and *V*<sub>2</sub> are the Verdet constants of the mixture, Ce(PO<sub>3</sub>)<sub>3</sub>, and Nd(PO<sub>3</sub>)<sub>3</sub>, respectively. Table III contains a list of

TABLE III. Sample concentration.

Sample number	Mole fraction	
	Ce (PO <sub>3</sub> ) <sub>3</sub>	Nd (PO <sub>3</sub> ) <sub>3</sub>
T 912-4	0	1
T 105-1	0.1	0.9
T 105-2	0.4	0.6
T 831-1	0.6	0.4
T 905-1	0.9	0.1
T 905-2	1	0

the samples with the respective mole fraction of the constituents.

The results of the Verdet constant measurements at room temperature are given in Table IV. The wavelength bandpass used resulted in an averaging of the

<sup>4</sup> N. J. Kreidl and J. R. Hensler, J. Am. Ceram. Soc. **38**, 423 (1955).

<sup>5</sup> C. K. Jorgensen, Mol. Phys. **5**, 271 (1962).

TABLE IV. Concentration dependence of the Verdet constant.

Sample $\lambda$ $m\mu$	-Verdet constant (min. of arc/cm Oe)									
	T 912-4 $E^a$	T 105-1 $E$ $C^a$		T 105-2 $E$ $C$		T 831-1 $E$ $C$		T 905-1 $E$ $C$		T 905-2 $E$
700	0.055	0.060	0.062	0.085	0.084	0.098	0.099	0.121	0.121	0.128
665	0.065	0.070	0.073	0.097	0.097	0.111	0.112	0.137	0.136	0.144
630	0.077	0.084	0.086	0.113	0.112	0.128	0.130	0.157	0.156	0.165
600	0.079	0.088	0.090	0.124	0.121	0.144	0.148	0.183	0.182	0.194
565	0.149	0.153	0.157	0.183	0.181	0.196	0.196	0.222	0.220	0.228
530	0.111	0.129	0.127	0.172	0.176	0.208	0.208	0.259	0.258	0.274
500	0.152	0.166	0.169	0.222	0.221	0.253	0.255	0.309	0.307	0.324
465	0.179	0.198	0.202	0.271	0.270	0.311	0.315	0.385	0.383	0.406
430	0.212	0.239	0.241	0.333	0.329	0.390	0.387	0.477	0.475	0.504

<sup>a</sup>  $E$ , experimental values;  $C$ , calculated values.

Verdet constant in the vicinity of the intra-f-orbital absorptions of  $Nd^{3+}$ . This averaging will make small changes of the Verdet constant difficult to detect in the absorption regions. Equation (3) was used to calculate Verdet constant values for the mixtures obtained by using the experimental values of  $V_1$  and  $V_2$ . The measured values are seen to be within 3.5% of the predicted values. With the measurement technique used, the experimental error decreased with decreasing wavelength (increasing rotation). A comparison of the predicted and measured values reflects this decrease in experimental error at the shorter wavelengths. For a single sample, the measured values tend to be systematically greater than or equal to, or less than or equal to the calculated values with the exception of a singular point within each sample. This consistency is attributed to a small error in the mole percent values.

Figure 2 contains a plot of the data in Table IV. The linear relation of the Verdet constant as a function of mole percent rare-earth phosphate is shown by the

close correspondence between the measured values and the straight lines of Eq. (3).

The room-temperature data thus indicate that the Verdet constant of the mixture is a linear function of the  $Ce^{3+}$  and  $Nd^{3+}$  concentrations. The same linearity was also found for the other rare-earth ion mixtures in various glass matrices. This result is consistent with the isolated nature of the 4f electrons and the relatively large distance between rare-earth ions which is calculated to be approximately 5.6 Å from the molecular weight and density on the basis of a hard-sphere model. The results indicate that higher Verdet constants are indeed feasible by using more condensed systems with respect to  $N$ . In fact, the highest value expected for  $N$  in a trivalent rare-earth ion insulator is approximately  $2 \times 10^{22}$  ions/cm<sup>3</sup> for  $R_2O_3$ , in other words 3 to 4 times the present values.

#### RARE-EARTH ION DEPENDENCE

Since the phosphate group does not contain any unpaired electrons in the ground state, the magnetic rotation due to this group will be diamagnetic (and positive) and is expected to be small. In addition, the concentration of phosphate is essentially constant. Therefore, the differences in the Verdet constants of the various glasses are attributed to the rare-earth ions.

Figure 3 contains a plot of the Verdet constant as a function of atomic number. In order to explain the observed variations, the equations of Van Vleck and Hebb<sup>6</sup> relating the Verdet constant and the magnetic susceptibility  $\chi$  for the rare-earth ions (except  $Sm^{3+}$  and especially  $Eu^{3+}$ ) will be used. Within the expressed conditions, these equations show that in addition to the established equality of temperature dependences,<sup>6-8</sup> certain conclusions concerning the magnitude of the Verdet constant with respect to the magnetic susceptibility are possible. These may be summarized by using the equations of Van Vleck and Hebb to obtain

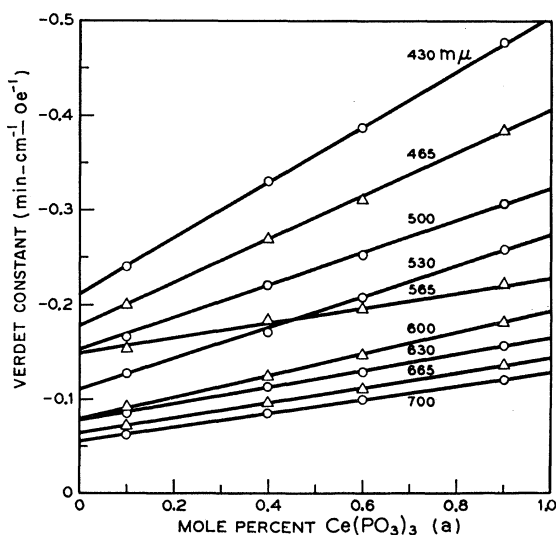


FIG. 2. Verdet constant as a function of mole percent  $Ce(PO_3)_3$  measured at selected incident light wavelengths. The straight lines are calculated from Eq. (3), and the measured values are denoted by circles and triangles.

<sup>6</sup> J. H. Van Vleck and M. H. Hebb, Phys. Rev. **46**, 17 (1934).

<sup>7</sup> S. B. Berger and C. B. Rubinstein (to be published).

<sup>8</sup> J. Becquerel, Commun. Kamerlingh Onnes Lab. Univ. Leiden No. 243d, 22 (1936).

(neglecting the diamagnetic rotation part)

$$V/\chi = (4\pi^2\nu^2 f/g\beta ch) \sum_{n'j'} C_{n'j'} \tau(n'j'; nj), \quad (4)$$

where  $\nu$  is the optical frequency,  $f=180 \times 60/\pi$  min/rad,  $g$  is the spectroscopic splitting factor,  $\beta$  is the Bohr magneton,  $c$  is the velocity of light in vacuum,  $h$  is Planck's constant, the  $C_{n'j'}$ 's are related to the transition probabilities (the indices  $j$  and  $j'$  denote, respectively, the ground and excited total angular momentum quantum numbers and  $n$  and  $n'$  signify all quantum numbers except for  $j$  and the magnetic quantum number  $m_j$ ) and  $\tau(n'j'; nj) = [\nu^2 - \nu(n'j'; nj)^2]^{-1}$ ; where  $\nu(n'j'; nj)$  is a transition frequency. Substituting for  $\chi$  according to (room-temperature approximation)<sup>9</sup>

$$\chi = Np^2\beta^2/3kT,$$

where  $N$  is the number of ions per cm<sup>3</sup>,  $p$  is the effective magneton number  $\{=g[J(J+1)]^{1/2}, J=j\}$ ,  $k$  is the Boltzmann constant, and  $T$  the absolute temperature, one obtains

$$V = A(Np^2/g) \sum_{n'j'} C_{n'j'} \tau(n'j'; nj), \quad (5)$$

where  $A = 4\pi^2\beta\nu^2 f/3chkT$ . The differences between Fig. 3 and the similar diagram, Fig. 4, for  $p^2/g$  (computed on the assumption that the multiplet splitting is large compared to  $kT$ ; invalid for Sm<sup>3+</sup> and Eu<sup>3+</sup>) are to be attributed to the variation in the summations of the

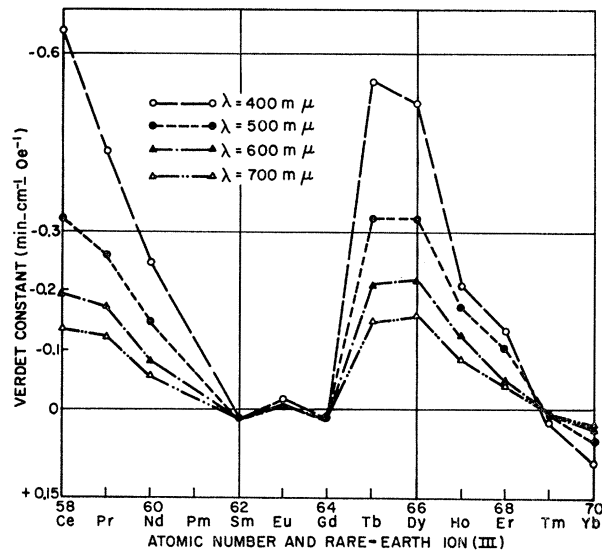


FIG. 3. Verdet constant of rare-earth (III) phosphate glasses measured at room temperature versus atomic number at an incident light wavelength of 700  $m\mu$ , 600  $m\mu$ , 500  $m\mu$ , and 400  $m\mu$ .

<sup>9</sup> Reference 3, pp. 242-244.

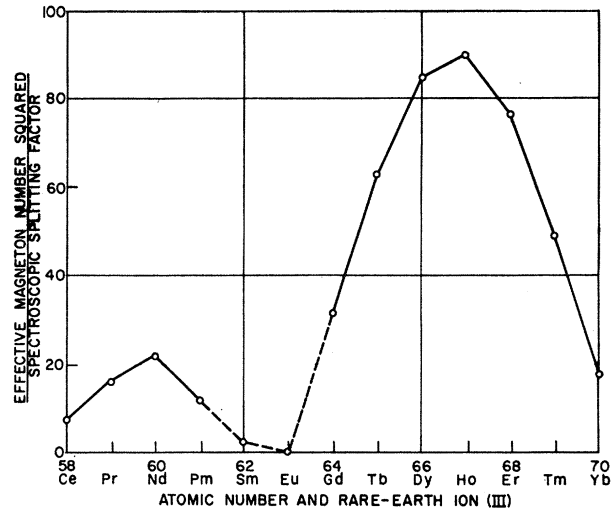


FIG. 4. Calculated effective magneton number squared divided by the spectroscopic splitting factor  $[=gJ(J+1)]$  presented as a function of atomic number of the trivalent rare-earth ions at room temperature.

$[C_{n'j'}\tau(n'j'; nj)]$ 's between the different rare-earth ions and in the  $N$ 's for our samples. As shown previously, the room-temperature data indicate that the Verdet constants for the rare-earth glasses are essentially linear in concentration, therefore, the major part of the differences is ascribable to the summations.

The transitions which are expected to be most instrumental in the rotation involve the promotion of a  $4f$  electron to the  $5d$  shell as can be surmised from the paper of Dieke, Crosswhite, and Dunn.<sup>10</sup> These authors show that the energy difference between the  $4f^n$  ( $n$ =number of electrons) ground state and  $4f^{n-1} 5d$  excited state increases with atomic number. This fact partially explains the variation of Verdet constant observed. The remainder of the variation must depend on the transitions and their matrix elements. It is evident that spectroscopic data pertaining to the allowed transitions of the rare-earth ions is very desirable in order that more quantitative statements concerning the differences between Figs. 3 and 4 can be made.

#### ACKNOWLEDGMENTS

The authors are indebted to M. D. Rigterink for his valuable discussions and encouragement of the program. In addition, the assistance of T. Kometani in the chemical analysis, J. J. McNicol in the magnetic rotation data, and Mrs. L. A. Baker in the density measurements is gratefully acknowledged.

<sup>10</sup> G. H. Dieke, H. M. Crosswhite, and B. Dunn, J. Am. Opt. Soc. 51, 820 (1961).